ACSNANO

www.acsnano.org

ARTICLE

Quantum Dot-Plasmon Lasing with Controlled Polarization Patterns

Jun Guan, Laxmi Kishore Sagar, Ran Li, Danqing Wang, Golam Bappi, Weijia Wang, Nicolas Watkins, Marc R. Bourgeois, Larissa Levina, Fengjia Fan, Sjoerd Hoogland, Oleksandr Voznyy, Joao Martins de Pina, Richard D. Schaller, George C. Schatz, Edward H. Sargent, and Teri W. Odom*

Cite This: https://dx.doi.org/10.1021/acsnano.9b09466

Read Online

ACCESS | Metrics & More | Article Recommendations | Supporting Information

ABSTRACT: The tailored spatial polarization of coherent light beams is important for applications ranging from microscopy to biophysics to quantum optics. Miniaturized light sources are needed for integrated, on-chip photonic devices with desired vector beams; however, this issue is unresolved because most lasers rely on bulky optical elements to achieve such polarization control. Here, we report on quantum dot-plasmon lasers with engineered polarization patterns controllable by near-field coupling of colloidal quantum dots to metal nanoparticles. Conformal coating of CdSe−CdS core−shell quantum dot films on Ag nanoparticle lattices enables the formation of hybrid waveguide-surface lattice resonance (W-SLR) modes. The sidebands of these hybrid modes at nonzero wavevectors facilitate directional lasing emission with either radial or azimuthal polarization depending on the thickness of the quantum dot film.

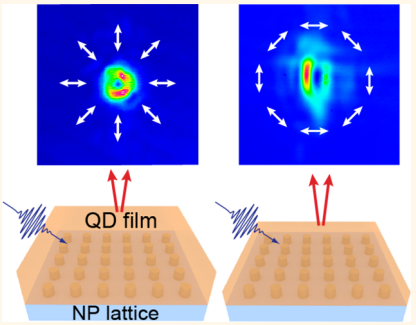

KEYWORDS: *lattice plasmons, surface lattice resonances, waveguide, band structure engineering, colloidal quantum dots, nanolaser, radially and azimuthally polarization states*

The polarization state of coherent light beams provides an important degree of freedom in photonic technologies.[1,2] In particular, radially and azimuthally polarized light can generate strong optical forces along the axial direction at the focal point, which is advantageous for optical trapping.[3,4] Also, radially polarized light can be focused to significantly smaller spot sizes than either linearly or circularly polarized beams,[5] which has enabled high-resolution imaging,[6] nanolithography,[7] and high-density optical memories.[8] Such cylindrical vector beams can be generated in different ways, such as combining two linearly polarized laser beams interferometrically,[9,10] passing a linearly polarized laser beam through a twisted nematic liquid crystal,[11,12] and inserting conical elements into a laser resonator.[13,14] These approaches rely on bulky optical components and their precise alignment, which has impeded widespread use in integrated optics. Although compact laser structures with radial and azimuthal polarization modes based on photonic crystals[15] or microring resonators[16] have been realized, the epitaxial semiconductors used as a gain medium are limited by high-temperature, high-vacuum, and stringent growth conditions. The realization of efficient, nanoscale light sources with desired polarization patterns requires simultaneous advances in both the gain materials and optical device design.

Colloidal quantum dots (QDs) are promising gain media because of high photoluminescence quantum yield and processability from solution phase.[17,18] Although QD lasing has been realized from whispering gallery modes,[19,20] by distributed feedback cavities,[21] by random scattering,[22] and from plasmonic modes,[23] control over the lasing polarization has not been possible. Plasmonic nanoparticle (NP) lattices represent an attractive nanocavity architecture in which the diffractive coupling between NPs produces surface lattice resonances (SLRs) with both high-quality factors and subwavelength mode confinement.[24−29] Engineering the band structure of SLR modes by refractive index, light polarization, and lattice geometry has facilitated nanoscale lasing with wavelengths that can be tuned in real time[30,31] and result in switchable, multimodal emission.[32,33] Closely packed QD layers can form high-refractive-index waveguides,[34] which provides an additional degree of freedom to manipulate the optical band structure of SLR modes. This hybrid nanomaterials system may control local light fields and also result in miniaturized, low-threshold coherent sources with tailored polarization patterns.

Received: December 1, 2019
Accepted: February 7, 2020

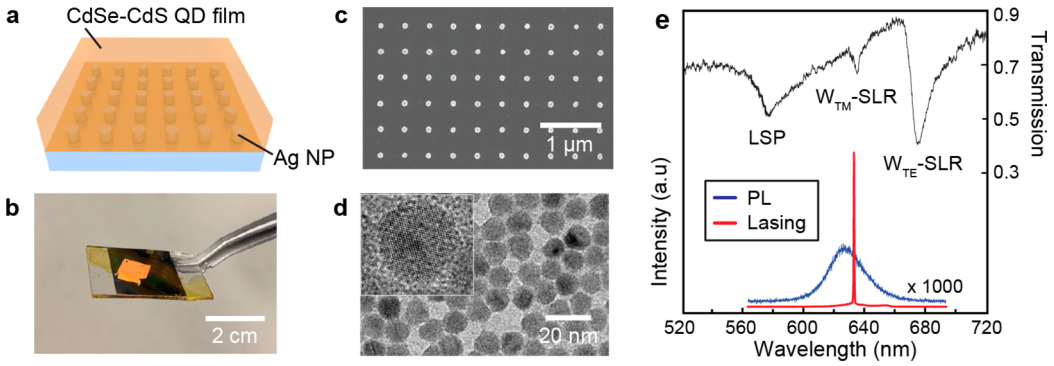

Figure 1. Design of QD-plasmon lasers. (a) Scheme of QD coating on top of Ag NP lattices with spacing a_0 = 400 nm. Ag NPs have dimensions with 70 nm diameter and 60 nm height and are scalable over cm^2 areas. The QD film is ~200 nm thick. (b) Photograph of QD film spin-coated on Ag NP lattices. (c) Scanning electron micrograph of Ag NPs lattice. (d) Transmission electron microscopy image of biaxially strained CdSe−CdS core−shell QDs. (e) Lasing observed where the photoluminescence of QDs overlapped with the hybrid waveguide-surface lattice resonance. Measured linear optical properties are in black; spontaneous emission of QD film without Ag NP lattice is in blue, and lasing emission of QD film on Ag NP lattice is in red.

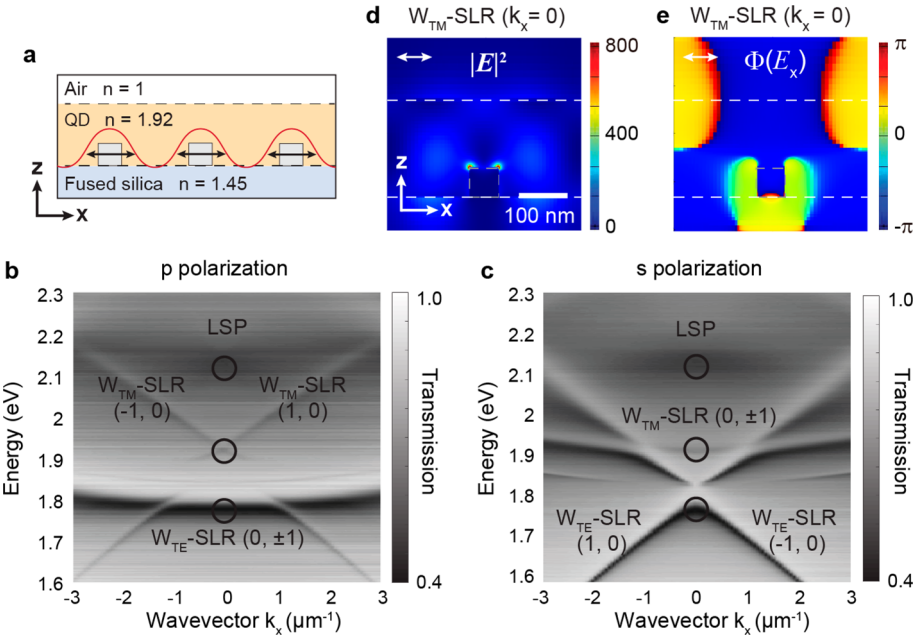

Figure 2. W-SLRs are produced due to hybridization of the optical waveguide formed by the high-index QD film and the surface lattice resonance excited in the Ag NP lattices. (a) Scheme of waveguide-surface lattice resonance coupling. Measured optical band structure of QD-plasmon device under (b) p- and (c) s-polarized light. Black circles indicate the W_{TE}-SLR, W_{TM}-SLR, and localized surface plasmon (LSP) modes at k_x = 0. (d) Simulated electric fields ($|E|^2$ with units of V^2 m^{-2}) and (e) phase distributions ($\varphi(E_x)$, with units of rad) at W_{TM}-SLR mode (k_x = 0). The electric field magnitude of the incident light E_0 was set as 1 V m^{-1} in the simulations.

Here, we show how hybrid waveguide-surface lattice resonance (W-SLR) modes can produce QD nanolasing with controlled polarization patterns. Based on modeling and measured materials parameters, we realized predicted structures whose near-field proximity of semiconductor QDs to plasmonic NPs resulted in electromagnetic couplings with polarization-dependent amplification. QD lasers were fabricated by conformally coating biaxially strained CdSe−CdS core−shell QDs on Ag NP lattices. These structures support W-SLR modes based on hybridization between the optical waveguide formed by the high-refractive-index QD film and the SLR excited in the Ag NP lattice. We demonstrate donut-shaped lasing patterns from the high-quality optical feedback supported at W-SLR sidebands at nonzero wavevectors. Either radially or azimuthally polarized lasing can be selected by changing the thickness of the QD film.

RESULTS AND DISCUSSION

Figure 1a,b represents nanolaser devices that integrate biaxially strained CdSe−CdS QDs with two-dimensional (2D) Ag NP lattices. First, we fabricated arrays of Ag NPs (spacing a_0 = 400 nm, diameter d = 70 nm, height h = 60 nm) (Figure 1c) using solvent-assisted nanoscale embossing (SANE[35]) and PEEL processes[36,37] over cm^2 areas (Methods section). Second, we synthesized biaxially strained, core−shell QDs *via* facet-selective epitaxy[38] (Figure 1d). These materials were produced by switching off, and then on, shell growth on the (0001) facet of wurtzite CdSe cores to produce asymmetric compressive shells with built-in biaxial strain while still maintaining surface passivation to avoid defects (Methods section). This synthesis procedure generates QDs having an exciton fine structure with sufficiently spaced hole states such that thermal depopulation

https://dx.doi.org/10.1021/acsnano.9b09466
ACS Nano XXXX, XXX, XXX−XXX

of valence band-edge states is prevented, resulting in lower optical gain thresholds.[38] Next we formed QD-plasmon devices by spin coating biaxially strained QDs on Ag NP lattices after identifying an optimized film thickness ($t \sim 200$ nm) for the desired cavity resonance wavelength, a design we achieved with the aid of finite-difference time-domain (FDTD) simulations (Figure S1 and the Methods section). Although two hybrid waveguide-SLR (W-SLR) modes are supported at visible wavelengths, we focused on the W_{TM}-SLR (λ = 635 nm, full-width-at-half-maximum (fwhm) = 4 nm) that overlaps with the photoluminescence (PL) of the QD film (Figure 1e). The feature at 580 nm showed localized surface plasmon (LSP) character influenced by the waveguide. The QD-plasmon device was optically pumped using 400 nm femtosecond (fs) pulses at room temperature, and emission spectra were collected normal to the sample surface (Methods section). Above a threshold pump intensity (~30 μJ cm^{-2}), a sharp and intense emission peak (λ_{lasing} = 633 nm, fwhm = 0.4 nm) emerged close to the wavelength of the W_{TM}-SLR mode. The lasing emission intensity was 3 orders of magnitude higher than the spontaneous emission.

Figure 2a depicts a scheme of the hybridized waveguide-SLR mode. The QD film formed an optical waveguide with a thickness t ~200 nm and a refractive index n ~1.92 (at $\lambda \sim$ 630 nm) (Figures S2 and S3) and was sandwiched between upper and lower media of air (n = 1.0) and fused silica (n = 1.45). The air/QD/silica stack supports a single transverse electric (TE) and a single transverse magnetic (TM) mode of different effective indices (Figure S4, calculated by electromagnetic mode treatment of a slab waveguide[39]). The periodic NP array provides the necessary momentum to couple surface plasmons to the TM and TE waveguide modes (Figure S4). We found that—in contrast with the case of SLRs supported by square lattices in a uniform n, where the NPs only couple in the direction orthogonal to the polarization of incident light[40]—the W-SLRs allow coupling of NPs in both orthogonal and parallel directions depending on the type of waveguide mode involved.

Figure 2b,c represents the optical band structure of the QD-NP lattice structure when the in-plane wavevector of incident light is along the x-direction (Methods section). W_{TE}-SLR modes resemble pure SLR modes:[25,41] one flat band follows the (0, ±1) diffraction order under p-polarized light, and two dispersive bands follow the (1, 0) and (−1, 0) diffraction orders under s-polarized light since NPs couple in the direction perpendicular to their dipole oscillations.[40] In contrast, we found that W_{TM}-SLR modes exhibit an inverse band structure, with two dispersive (1, 0) and (−1, 0) bands under p-polarized illumination and one flat (0, ±1) band under s-polarized illumination (Figure 2b); hence, facilitated by the TM waveguide mode, the Ag NPs can be strongly coupled along the direction parallel to their dipole moments (Figure S5). We simulated the near-field properties of the band-edge at $k_x = 0$ to visualize the plasmonic and waveguide features of the hybrid W_{TM}-SLR mode (Figure 2d). Strong electric field enhancement ($|E|^2/|E_0|^2 > 800$) at the top edges of the Ag NPs results from coherent interactions between the NPs. The phase change at the top surface of the QD film indicates total internal reflection at the boundary between the high-index film and air (Figure 2e).

To determine how W-SLR modes can provide feedback for lasing, we photoexcited the QD-plasmon device using 35 fs, 400 nm laser pulses at room temperature and collected the emission spectra normal to the sample surface (Methods section). Ultrashort pulses are advantageous to generate biexcitons in QDs on time scales that are faster than Auger recombination (100−1,000 ps)[42] for efficient excitation of optical gain. At low pump intensities (<30 μJ cm^{-2}), the emission exhibited a PL profile (fwhm ~7 nm) that was spectrally modified by the W-SLR mode (Figure 3a, Figure S6). Above a critical pump intensity (~30 μJ cm^{-2}), a sharp and intense emission peak (λ = 633 nm, fwhm = 0.4 nm) emerged close to the position of the W_{TM}-SLR (λ = 635 nm, fwhm = 4 nm). The pump energy versus output intensity curve on a log−log scale showed an S-shaped threshold behavior: (1) The PL intensity first increased linearly because the rate of photon losses exceeded the rate of stimulated emission. (2) Above threshold, the lasing intensity experienced a transition region with superlinear growth. (3) At high pump powers, the slope of the input−output curve decreased because of saturation of biexciton population.[43,44] As a control experiment to verify the importance of the plasmonic NP lattices for optical feedback, we spin-cast a QD film with the same thickness on a fused silica substrate. In the absence of the Ag NP lattice, only amplified spontaneous emission (ASE) was observed from the waveguide mode with a larger linewidth (fwhm ~ 10 nm) and lower intensity (Figure S7).

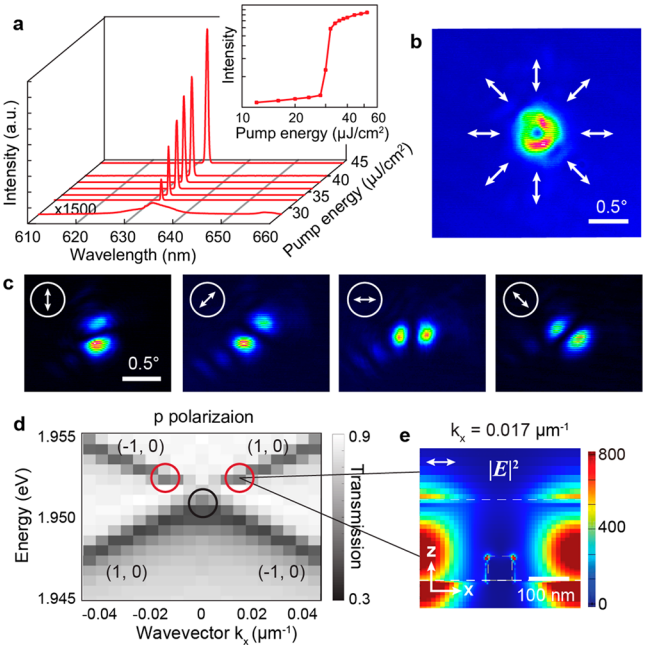

Figure 3. Radially polarized QD lasing was achieved from hybrid W_{TM}-SLR nanocavities. (a) Emission spectra collected at the normal detection angle for different input pump pulse energies on a linear scale. Inset: output emission intensity as a function of input pump pulse energy on a log−log scale. (b) Far-field pattern of lasing emission beam. White arrows show the polarization direction of the output lasing pattern. (c) Beam profiles under selected polarization directions. White arrows show the polarization direction of the linear polarizer in front of the detector. (d) Simulated band structure at small wavevectors under p-polarized light. The black circle indicates the W_{TM}-SLR mode at $k_x = 0$. The red circles indicate the W_{TM}-SLR sidebands at nonzero k_x. (e) Simulated electric fields ($|E|^2$ with units of V^2 m^{-2}) at the W_{TM}-SLR sidebands. The electric field magnitude of the incident light E_0 was set as 1 V m^{-1} in the simulations.

https://dx.doi.org/10.1021/acsnano.9b09466
ACS Nano XXXX, XXX, XXX−XXX

When we mapped the far-field pattern of emitted light using a charge coupled device (CCD) beam profiler, we observed a donut-shaped emission beam with small divergence angle (<0.5°) (Figure 3b). To study the shape further, we captured the lasing signal at selected polarization directions by rotating a linear polarizer in front of the detector (Figure 3c). The images showed two lobes that followed the rotation of the polarizer, which indicates that the QD lasing was radially polarized. To determine the origin of the donut-shaped emission, we simulated the optical band structure with small step sizes in wavevector ($\Delta k_x \sim 0.005\ \mu m^{-1}$) and energy ($\Delta E \sim 0.0006$ eV) (Figure 3d) using the FDTD method and found that two flat sidebands formed at small k_x with energy slightly higher than the resonance at $k_x = 0$. (Note: in experiments, these W_{TM}-SLR sidebands at $\theta \sim 0.1°$ are included in our zero-degree transmission spectrum because of the relatively large collection angle (~0.5°) of our CCD detector.) The near-zero group velocities at small nonzero wavevectors indicate that these sidebands can trap photons and provide optical feedback for lasing. Compared to the resonance at $k_x = 0$ (Figure 2d), the sidebands (Figure 3e, Figures S8 and S9) showed strong electric field enhancement in both the hotspot regions around the NPs and within the bulk region between NPs. Hence, a larger volume of QDs experience emission enhancement by the sideband modes, which can lead to stronger emission at off-normal angles and suppression of the W_{TM}-SLR mode at $k_x = 0$. We note that, because of the symmetry of the square lattice, a similar analysis can be applied to the W_{TM}-SLR sideband modes at nonzero k_y.

In contrast to the radially polarized beam in Figure 3c, previous reports of SLR lasing using dye molecules as the gain media showed linear polarization with an elongated Gaussian intensity distribution.[30,32,45] Since the linearly polarized pump laser preferentially excites dye molecules whose 1D transition dipole moments are oriented parallel to the pump polarization, only the SLR mode perpendicular to that direction can provide optical feedback, which results in linearly polarized SLR lasing. Different from dye molecules, the transition dipole moment of a QD is degenerate in the plane perpendicular to the crystal axis.[46,47] Independent of the polarization of the excitation light, the emission from a QD exhibits random polarization in the 2D plane of the transition dipole.[46,47] Therefore, emission from a layer of randomly oriented QDs enables excitation of W_{TM}-SLR modes along both axes of the plasmonic NP lattice (x- and y-directions) regardless of pump polarization. This simultaneous excitation of W_{TM}-SLR sidebands at nonzero k_x and nonzero k_y resulted in a donut-shaped lasing profile (Figure 3b,c, Figure S10). Both the emission properties of QDs and the 2D plasmonic NP lattice are critical in realizing lasing polarization patterns with circular symmetry under a linear pump.

We examined energy transfer between excitations in QDs and W-SLR cavity modes by measuring the time response of W_{TM}-SLR lasing using a streak camera (Figure 4, Figure S11, and the Methods section). Below the lasing threshold, modified PL from the QD film on the Ag NP lattice exhibited a long decay lifetime (~3 ns) (Figure S11) from single exciton emission. Above threshold, the decay lifetime of excited states was significantly reduced to ~10 ps since the biexciton population is quickly depleted by the stimulated emission. We discovered that lasing had a rise time between the pump pulse and the lasing emission on the order of tens of picoseconds, much longer than that of ASE from a QD waveguide without a

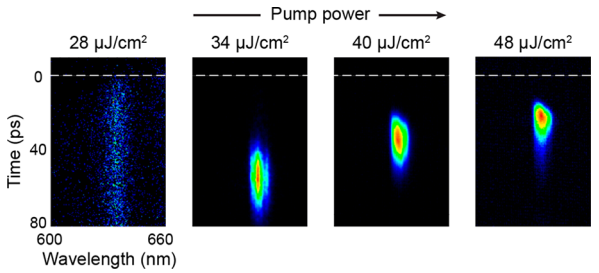

Figure 4. Rise time and decay lifetime of QD nanolasing demonstrate the energy transfer between QD biexcitons and W_{TM}-SLR cavity modes. Time-resolved streak camera images of QD emission on Ag NP lattices at 28, 34, 40, and 48 μJ cm^{-2}.

NP lattice (Figures S12 and S13). The rise time reveals that although optical gain in QDs builds up instantaneously (<1 ps),[48] the depletion of population inversion is a gradual process because of interactions of QDs with the optical cavity, consistent with a three-state QD lasing model.[43] During this delay period, spontaneous emission of QD biexcitons excites plasmons, which then in turn enhance the spontaneous and stimulated emission rates of the biexcitons. The onset of lasing occurs when stimulated emission outcompetes photon losses in the W_{TM}-SLR cavity and nonradiative Auger losses in the QDs. We found that increasing the pump power is an effective approach to decrease the rise time of QD-plasmon lasers (Figure 4 and Figure S13) because higher excitation intensities can increase the stimulated emission rates of QDs and facilitate faster energy transfer between biexcitons and plasmons. To understand the carrier dynamics in QDs, we measured the decay lifetime of lasing from a QD layer on Ag NP lattices and the lifetime of ASE from a pure QD layer without NP lattices. We found that both decay lifetimes were comparable (Figures S12 and S13), which indicates that optical confinement from the high-refractive-index waveguide is more critical than plasmons for modifying biexciton lifetimes in stimulated emission.

To obtain azimuthally polarized lasing output, we changed the thickness of the QD film so that the QD emission overlapped with the sidebands of the W_{TE}-SLR mode. Because varying the thickness of the QD film can modulate the effective refractive index of the waveguide mode,[39] the wavelengths of hybrid W_{TE}-SLR and W_{TM}-SLR modes can be tuned. We decreased the film thickness from 200 to 150 nm (Figure S14), which shifted the resonances to shorter wavelengths so that only W_{TE}-SLR sidebands (644 nm) overlapped with the QD emission; the W_{TM}-SLR sidebands (615 nm) were now beyond the PL envelope (Figure S15).

The W_{TE}-SLR showed a large band gap (~0.1 eV; 20 nm) between the upper two sidebands and the lower single band (Figure 5a). We observed that the lasing wavelength (λ = 645 nm) was very close to the upper band wavelengths (λ = 644 nm) (Figure 5b), which unambiguously demonstrates in experiment that the optical feedback is provided by W_{TE}-SLR sidebands. (Note: since the W_{TE}-SLR sidebands are excited at ±1° incident angles, these resonances can be captured separately by our CCD detector, and which validates the simulation result of W_{TM}-SLR sidebands for radial polarization in Figure 3.) In the lasing process, although QDs emit photons with random polarization directions, only those photons whose energy (E), in-plane wavevector ($\mathbf{k}_{//}$), and polarization (s or p) match the excitation conditions of W-

https://dx.doi.org/10.1021/acsnano.9b09466
ACS Nano XXXX, XXX, XXX−XXX

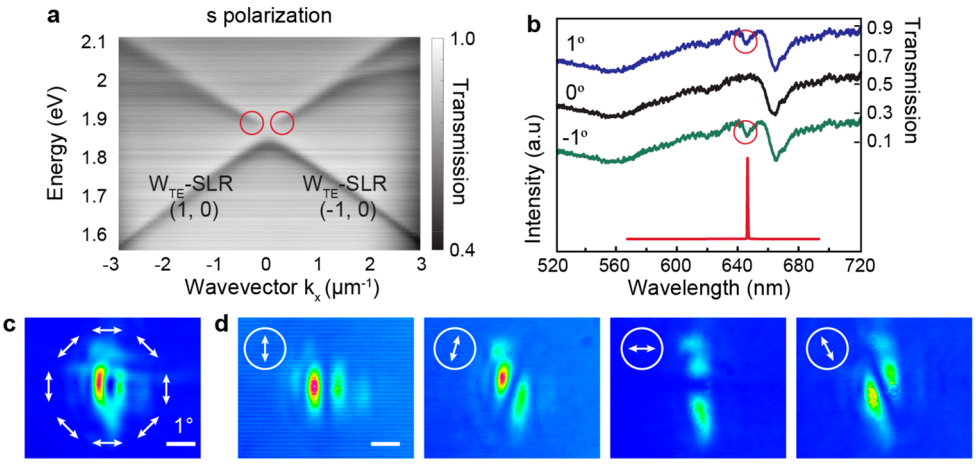

Figure 5. Engineering of lasing polarization by varying QD film thickness. (a) Measured optical band structure of the QD-plasmon device under s-polarized light. The QD film is ∼150 nm thick. Red circles indicate the sidebands of the W_{TE}-SLR modes. (b) Measured transmission spectra of the QD-plasmon device with incident angles −1° (green), 0° (black), 1° (blue), and measured lasing spectrum (red) normal to the lattice surface. Transmission spectra at 0° and −1° were shifted down 0.3 and 0.6, respectively, for clarity. The collection angle for the lasing spectrum is ∼3°. (c) Far-field pattern of lasing emission beam. White arrows show the polarization direction of the output lasing pattern. (d) Beam profiles under selected polarization directions. White arrows show the polarization direction of the linear polarizer in front of the detector.

SLR sidebands can efficiently build up in the W-SLR cavity mode. In contrast to the W_{TM}-SLR mode, whose sidebands are excited under p-polarized light, the W_{TE}-SLR mode shows sidebands under s-polarized light (Figure S15). Therefore, the W_{TE}-SLR sidebands with s-polarized excitation condition can support an azimuthally polarized lasing beam (Figure 5c and Figure S16). Compared to the W_{TM}-SLR mode, the emission from the W_{TE}-SLR modes had a larger divergence angle (∼1.5°), which is consistent with the larger separation between the sidebands in k space.

CONCLUSIONS

In summary, we realized QD-plasmon nanolasing with engineered polarization patterns using waveguide-SLR cavity modes. The hybridization of waveguide modes and SLR modes facilitated lasing beams from flat modes at nonzero wavevectors. Either radially or azimuthally polarized lasing can be achieved by controlling which W-SLR mode overlaps with QD emission. Compared to current techniques that place bulk optical components outside or inside a macroscale laser cavity for polarization control, we have realized a miniaturized materials system that can generate desired polarization patterns from nanoscale laser sources. Looking forward, we expect that more complex light beams with controlled intensity, polarization, and phase can be achieved by engineering W-SLR band structure through the design of lattice symmetry and unit cells and choice of gain. Controlling nanoscale energy transfer between QDs and W-SLR modes offers prospects for hybrid QD-plasmon systems in quantum communication and information applications.

METHODS

Fabrication of Ag NP Lattices. Ag NP lattices on fused silica were fabricated with a soft nanofabrication process. First, we generated periodic photoresist posts on Si wafers by solvent-assisted nanoscale embossing (SANE[35]). After Cr deposition (8 nm), liftoff of photoresist posts, Si etching (300 nm), and Au deposition (80 nm), Au nanohole films were produced on the Si substrate with a Cr adhesion layer in between. Wet etching the Cr layer released the Au nanohole film from the Si wafer. The Au film was then floated on water and transferred to a fused silica substrate. After deposition of 2 nm Cr and 60 nm Ag through the Au hole film, followed by removal of the Au hole film with tape, Ag NP lattices were patterned on the silica substrate. (The 2 nm Cr layer was used to improve adhesion between Ag NPs and silica.) A 5 nm Al_2O_3 layer was deposited on top of Ag NP lattices to prevent oxidation and sulfidation of Ag.

Synthesis of Colloidal QDs. CdSe colloidal QDs were synthesized using the existing literature protocol.[49,50] Biaxially strained asymmetric core/shell QDs synthesis, purification, and chloride ligand exchanges were done by following a previously published report.[38,49,50]

Fabrication of QD-Plasmon Laser. First, Ag NP lattices on fused silica were cleaned by oxygen plasma for 5 min. Then, the Cl-exchanged biaxially strained QDs were spin-cast onto the Ag NPs at a spin speed of 500−2000 rpm for 60 s. The thickness of the QD film was controlled by the concentration of the QD solution and the spin-coating speed. Diluting the QD solution or decreasing the spin-coating speed resulted in a thinner QD film.

Band Structure Measurements. The optical band structure of QD-Ag NP lattices was obtained by measuring transmission spectra at different incident angles. A collimated white light from a halogen lamp was used to illuminate the samples. The transmitted light was collected at the backside of the sample. The background spectrum without the sample was recorded as a reference to calculate the transmission efficiency. The rotation of the samples was controlled by a program-controlled stage to change the incident angles. By collecting the transmission spectra from incident angles −30° to 30° in 0.5° increments, band structures of the QD-Ag NP lattices in wavelength (λ)−incident angle (θ) units was obtained. Band structure in energy (E)−wavevector ($k_{//}$) format was plotted by converting the $\lambda-\theta$ relation to the $E-k_{//}$ relation based on $E = hc/\lambda$ and $k_{//} = (2\pi/\lambda)\sin\theta$.

FDTD Simulations. The linear optical properties of QD-Ag NP lattices were simulated by FDTD calculations using commercial software (FDTD solution, Lumerical Inc., Vancouver, Canada). In the x- and y-directions, Bloch boundary conditions were applied to simulate infinite lattices. In the z-direction, perfectly matched layer (PML) boundary conditions were used to absorb the light waves. The silica substrate (n = 1.45) for the Ag NP lattices occupied the lower half of the simulation box while the refractive index on top of the QD layer was set to be 1.0. The optical constants of Ag were taken from the CRC handbook.[51] The QD layer was simulated by a dielectric model where the material has a specified index n = 1.92 at all frequencies. A uniform mesh size of 4 nm (x-, y-, and z-directions)

https://dx.doi.org/10.1021/acsnano.9b09466
ACS Nano XXXX, XXX, XXX−XXX

surrounding the Ag NPs ensures accurate calculations of electromagnetic fields.

Lasing Measurements. The QD-plasmon laser was optically pumped at room temperature using 35 fs, 400 nm laser pulses with a repetition rate of 1 kHz and beam diameter of ~500 μm. The 400 nm laser pulses were generated through an optical parametric amplifier using a Ti:sapphire laser. Lasing signals were collected normal to the lattice plane and analyzed by a spectrometer and CCD camera. The resolution of the spectrometer is 0.1 nm. Decreasing the slit width of the spectrometer could slightly improve the resolution at a cost of collection efficiency. The far-field emission patterns were collected by a high-resolution CCD beam profiler.

Time-Resolved Emission Dynamics. Power-dependent lasing dynamics were characterized by a streak camera. The QD-plasmon laser was optically pumped at room temperature by 35 fs, 400 nm laser pulses generated through an optical parametric amplifier using a Ti:sapphire laser. After the emission signals passed through a long-pass (550 nm) and neutral density filter, the photons were coupled to an optical fiber, directed to a spectrometer, and collected by a single-photon-sensitive streak camera. An exponential decay function $y = y_0 + Ae^{-(x - x_0)/t}$ was used to fit the emission intensities and obtain emission decay lifetime t.

ASSOCIATED CONTENT

Supporting Information

The Supporting Information is available free of charge at https://pubs.acs.org/doi/10.1021/acsnano.9b09466.

> Dependence of W-SLR modes on the thickness of the QD film; thickness and refractive index of the QD film; hybridization of waveguide modes and SLR modes; nanoparticle coupling direction for W_{TE}-SLR and W_{TM}-SLR modes; angle-resolved photoluminescence from the QD film on Ag NP lattices; amplified spontaneous emission from the QD film; electric field distribution and phase map of W_{TM}-SLR sidebands; dielectric NP lattices in the air/QD/silica waveguide structure; beam profiles under different pump polarization; dynamics of quantum dot-plasmon lasing; comparison of the dynamics of lasing and amplified spontaneous emission; coherent lasing action from W_{TE}-SLR mode; and engineering optical band structure by the thickness of the QD film (PDF)

AUTHOR INFORMATION

Corresponding Author

Teri W. Odom − *Graduate Program in Applied Physics, Department of Materials Science and Engineering, and Department of Chemistry, Northwestern University, Evanston, Illinois 60208, United States;* orcid.org/0000-0002-8490-292X; Email: todom@northwestern.edu

Authors

Jun Guan − *Graduate Program in Applied Physics, Northwestern University, Evanston, Illinois 60208, United States;* orcid.org/0000-0001-8667-1611

Laxmi Kishore Sagar − *Department of Electrical and Computer Engineering, University of Toronto, Toronto, Ontario M5S 3G4, Canada*

Ran Li − *Department of Materials Science and Engineering, Northwestern University, Evanston, Illinois 60208, United States;* orcid.org/0000-0001-5606-3826

Danqing Wang − *Graduate Program in Applied Physics, Northwestern University, Evanston, Illinois 60208, United States;* orcid.org/0000-0002-7369-1944

Golam Bappi − *Department of Electrical and Computer Engineering, University of Toronto, Toronto, Ontario M5S 3G4, Canada*

Weijia Wang − *Graduate Program in Applied Physics, Northwestern University, Evanston, Illinois 60208, United States*

Nicolas Watkins − *Department of Chemistry, Northwestern University, Evanston, Illinois 60208, United States*

Marc R. Bourgeois − *Department of Chemistry, Northwestern University, Evanston, Illinois 60208, United States*

Larissa Levina − *Department of Electrical and Computer Engineering, University of Toronto, Toronto, Ontario M5S 3G4, Canada*

Fengjia Fan − *Department of Electrical and Computer Engineering, University of Toronto, Toronto, Ontario M5S 3G4, Canada*

Sjoerd Hoogland − *Department of Electrical and Computer Engineering, University of Toronto, Toronto, Ontario M5S 3G4, Canada*

Oleksandr Voznyy − *Department of Electrical and Computer Engineering, University of Toronto, Toronto, Ontario M5S 3G4, Canada;* orcid.org/0000-0002-8656-5074

Joao Martins de Pina − *Department of Electrical and Computer Engineering, University of Toronto, Toronto, Ontario M5S 3G4, Canada*

Richard D. Schaller − *Department of Chemistry, Northwestern University, Evanston, Illinois 60208, United States; Center for Nanoscale Materials, Argonne National Laboratory, Lemont, Illinois 60439, United States;* orcid.org/0000-0001-9696-8830

George C. Schatz − *Graduate Program in Applied Physics and Department of Chemistry, Northwestern University, Evanston, Illinois 60208, United States;* orcid.org/0000-0001-5837-4740

Edward H. Sargent − *Department of Electrical and Computer Engineering, University of Toronto, Toronto, Ontario M5S 3G4, Canada;* orcid.org/0000-0003-0396-6495

Complete contact information is available at: https://pubs.acs.org/10.1021/acsnano.9b09466

Author Contributions

J.G. and T.W.O. conceived the idea of QD-plasmon nanolasing with controlled polarization patterns. J.G. fabricated the Ag NP lattices, characterized the linear optical properties of the QD-plasmon devices, carried out the lasing measurements, and performed the FDTD numerical simulations. L.K.S., G.B., L.L., F.F., S.H., O.V., and J.M.P. synthesized the colloidal QDs. R.L., W.W., and N.W. contributed to the lasing measurements. D.W. and M.R.B. contributed to data interpretation. T.W.O., E.H.S., G.C.S., and R.D.S. guided the experimental and theoretical investigations. J.G. and T.W.O. analyzed the data and wrote the manuscript. All authors commented on and revised the manuscript.

Notes

The authors declare no competing financial interest.

ACKNOWLEDGMENTS

This work was supported by the National Science Foundation (NSF) under DMR-1608258, DMR-1904385, and the Vannevar Bush Faculty Fellowship from DOD under N00014-17-1-3023. This work used the Northwestern University Micro/Nano Fabrication Facility (NUFAB), which is partially supported by Soft and Hybrid Nanotechnology Experimental (SHyNE) Resource (NSF ECCS-1542205), the Materials Research Science and Engineering

Center (MRSEC) (DMR-1720139), the State of Illinois, and Northwestern University. This work made use of the EPIC, SPID, and Keck-II facilities of Northwestern University's NUANCE Center, which has received support from the SHyNE Resource (NSF ECCS-1542205), the MRSEC program (NSF DMR-1720139) at the Materials Research Center, the International Institute for Nanotechnology (IIN), the Keck Foundation, and the State of Illinois through the IIN. This research was supported in part by the Quest high performance computing facility at Northwestern University, which is jointly supported by the Office of the Provost, the Office for Research, and Northwestern University Information Technology. This research was supported by the Ontario Research Fund—Research Excellence Program and by the Natural Sciences and Engineering Research Council (NSERC) of Canada. We thank Dr. Charles Cherqui and Dr. Dhara Trivedi for discussions.

REFERENCES

(1) Rubinsztein-Dunlop, H.; Forbes, A.; Berry, M. V.; Dennis, M. R.; Andrews, D. L.; Mansuripur, M.; Denz, C.; Alpmann, C.; Banzer, P.; Bauer, T.; Karimi, E.; Marrucci, L.; Padgett, M.; Ritsch-Marte, M.; Litchinitser, N. M.; Bigelow, N. P.; Rosales-Guzman, C.; Belmonte, A.; Torres, J. P.; Neely, T. W.; et al. Roadmap on Structured Light. *J. Opt. (Bristol, U. K.)* **2017**, *19*, No. 013001.

(2) Zhan, Q. W. Cylindrical Vector Beams: From Mathematical Concepts to Applications. *Adv. Opt. Photonics* **2009**, *1*, 1−57.

(3) Kozawa, Y.; Sato, S. Optical Trapping of Micrometer-Sized Dielectric Particles by Cylindrical Vector Beams. *Opt. Express* **2010**, *18*, 10828−10833.

(4) Zhan, Q. W. Trapping Metallic Rayleigh Particles with Radial Polarization. *Opt. Express* **2004**, *12*, 3377−3382.

(5) Dorn, R.; Quabis, S.; Leuchs, G. Sharper Focus for a Radially Polarized Light Beam. *Phys. Rev. Lett.* **2003**, *91*, 233901.

(6) Chen, R.; Agarwal, K.; Sheppard, C. J. R.; Chen, X. D. Imaging Using Cylindrical Vector Beams in a High-Numerical-Aperture Microscopy System. *Opt. Lett.* **2013**, *38*, 3111−3114.

(7) Helseth, L. E. Roles of Polarization, Phase and Amplitude in Solid Immersion Lens Systems. *Opt. Commun.* **2001**, *191*, 161−172.

(8) Kim, W. C.; Park, N. C.; Yoon, Y. J.; Choi, H.; Park, Y. P. Investigation of Near-Field Imaging Characteristics of Radial Polarization for Application to Optical Data Storage. *Opt. Rev.* **2007**, *14*, 236−242.

(9) Tidwell, S. C.; Ford, D. H.; Kimura, W. D. Generating Radially Polarized Beams Interferometrically. *Appl. Opt.* **1990**, *29*, 2234−2239.

(10) Wang, X. L.; Ding, J. P.; Ni, W. J.; Guo, C. S.; Wang, H. T. Generation of Arbitrary Vector Beams with a Spatial Light Modulator and a Common Path Interferometric Arrangement. *Opt. Lett.* **2007**, *32*, 3549−3551.

(11) Stalder, M.; Schadt, M. Linearly Polarized Light with Axial Symmetry Generated by Liquid-Crystal Polarization Converters. *Opt. Lett.* **1996**, *21*, 1948−1950.

(12) Maurer, C.; Jesacher, A.; Furhapter, S.; Bernet, S.; Ritsch-Marte, M. Tailoring of Arbitrary Optical Vector Beams. *New J. Phys.* **2007**, *9*, 78.

(13) Yonezawa, K.; Kozawa, Y.; Sato, S. Generation of a Radially Polarized Laser Beam by Use of the Birefringence of a C-Cut Nd: Yvo4 Crystal. *Opt. Lett.* **2006**, *31*, 2151−2153.

(14) Kozawa, Y.; Sato, S. Generation of a Radially Polarized Laser Beam by Use of a Conical Brewster Prism. *Opt. Lett.* **2005**, *30*, 3063−3065.

(15) Miyai, E.; Sakai, K.; Okano, T.; Kunishi, W.; Ohnishi, D.; Noda, S. Photonics: Lasers Producing Tailored Beams. *Nature* **2006**, *441*, 946−946.

(16) Miao, P.; Zhang, Z. F.; Sun, J. B.; Walasik, W.; Longhi, S.; Litchinitser, N. M.; Feng, L. Orbital Angular Momentum Microlaser. *Science* **2016**, *353*, 464−467.

(17) Talapin, D. V.; Lee, J. S.; Kovalenko, M. V.; Shevchenko, E. V. Prospects of Colloidal Nanocrystals for Electronic and Optoelectronic Applications. *Chem. Rev.* **2010**, *110*, 389−458.

(18) Wang, Y.; Sun, H. D. Advances and Prospects of Lasers Developed from Colloidal Semiconductor Nanostructures. *Prog. Quantum Electron.* **2018**, *60*, 1−29.

(19) Malko, A. V.; Mikhailovsky, A. A.; Petruska, M. A.; Hollingsworth, J. A.; Htoon, H.; Bawendi, M. G.; Klimov, V. I. From Amplified Spontaneous Emission to Microring Lasing Using Nanocrystal Quantum Dot Solids. *Appl. Phys. Lett.* **2002**, *81*, 1303−1305.

(20) Fan, X. D.; Palinginis, P.; Lacey, S.; Wang, H. L.; Lonergan, M. C. Coupling Semiconductor Nanocrystals to a Fused-Silica Microsphere: A Quantum-Dot Microcavity with Extremely High Q Factors. *Opt. Lett.* **2000**, *25*, 1600−1602.

(21) Roh, K.; Dang, C.; Lee, J.; Chen, S. T.; Steckel, J. S.; Coe-Sullivan, S.; Nurmikko, A. Surface-Emitting Red, Green, and Blue Colloidal Quantum Dot Distributed Feedback Lasers. *Opt. Express* **2014**, *22*, 18800−18806.

(22) Gollner, C.; Ziegler, J.; Protesescu, L.; Dirin, D. N.; Lechner, R. T.; Fritz-Popovski, G.; Sytnyk, M.; Yakunin, S.; Rotter, S.; Amin, A. A. Y.; Vidal, C.; Hrelescu, C.; Klar, T. A.; Kovalenko, M. V.; Heiss, W. Random Lasing with Systematic Threshold Behavior in Films of Cdse/Cds Core/Thick-Shell Colloidal Quantum Dots. *ACS Nano* **2015**, *9*, 9792−9801.

(23) Kress, S. J. P.; Cui, J.; Rohner, P.; Kim, D. K.; Antolinez, F. V.; Zaininger, K. A.; Jayanti, S. V.; Richner, P.; McPeak, K. M.; Poulikakos, D.; Norris, D. J. A Customizable Class of Colloidal-Quantum-Dot Spasers and Plasmonic Amplifiers. *Sci. Adv.* **2017**, *3*, No. e1700688.

(24) Yang, A.; Hryn, A. J.; Bourgeois, M. R.; Lee, W.-K.; Hu, J.; Schatz, G. C.; Odom, T. W. Programmable and Reversible Plasmon Mode Engineering. *Proc. Natl. Acad. Sci. U. S. A.* **2016**, *113*, 14201−14206.

(25) Wang, W. J.; Ramezani, M.; Vakevainen, A. I.; Torma, P.; Rivas, J. G.; Odom, T. W. The Rich Photonic World of Plasmonic Nanoparticle Arrays. *Mater. Today* **2018**, *21*, 303−314.

(26) Zou, S. L.; Janel, N.; Schatz, G. C. Silver Nanoparticle Array Structures That Produce Remarkably Narrow Plasmon Lineshapes. *J. Chem. Phys.* **2004**, *120*, 10871−10875.

(27) Auguie, B.; Barnes, W. L. Collective Resonances in Gold Nanoparticle Arrays. *Phys. Rev. Lett.* **2008**, *101*, 143902.

(28) Li, R.; Bourgeois, M. R.; Cherqui, C.; Guan, J.; Wang, D. Q.; Hu, J. T.; Schaller, R. D.; Schatz, G. C.; Odom, T. W. Hierarchical Hybridization in Plasmonic Honeycomb Lattices. *Nano Lett.* **2019**, *19*, 6435−6441.

(29) Wang, D.; Guan, J.; Hu, J.; Bourgeois, M. R.; Odom, T. W. Manipulating Light−Matter Interactions in Plasmonic Nanoparticle Lattices. *Acc. Chem. Res.* **2019**, *52*, 2997−3007.

(30) Yang, A. K.; Hoang, T. B.; Dridi, M.; Deeb, C.; Mikkelsen, M. H.; Schatz, G. C.; Odom, T. W. Real-Time Tunable Lasing from Plasmonic Nanocavity Arrays. *Nat. Commun.* **2015**, *6*, 6939.

(31) Wang, D.; Bourgeois, M. R.; Lee, W. K.; Li, R.; Trivedi, D.; Knudson, M. P.; Wang, W.; Schatz, G. C.; Odom, T. W. Stretchable Nanolasing from Hybrid Quadrupole Plasmons. *Nano Lett.* **2018**, *18*, 4549−4555.

(32) Wang, D.; Yang, A.; Wang, W.; Hua, Y.; Schaller, R. D.; Schatz, G. C.; Odom, T. W. Band-Edge Engineering for Controlled Multi-Modal Nanolasing in Plasmonic Superlattices. *Nat. Nanotechnol.* **2017**, *12*, 889−894.

(33) Knudson, M. P.; Li, R.; Wang, D. Q.; Wang, W. J.; Schaller, R. D.; Odom, T. W. Polarization-Dependent Lasing Behavior from Low-Symmetry Nanocavity Arrays. *ACS Nano* **2019**, *13*, 7435−7441.

(34) Klimov, V. I.; Mikhailovsky, A. A.; Xu, S.; Malko, A.; Hollingsworth, J. A.; Leatherdale, C. A.; Eisler, H. J.; Bawendi, M. G. Optical Gain and Stimulated Emission in Nanocrystal Quantum Dots. *Science* **2000**, *290*, 314−317.

https://dx.doi.org/10.1021/acsnano.9b09466
ACS Nano XXXX, XXX, XXX−XXX

(35) Lee, M. H.; Huntington, M. D.; Zhou, W.; Yang, J.-c.; Odom, T. W. Programmable Soft Lithography: Solvent-Assisted Nanoscale Embossing. *Nano Lett.* **2011**, *11*, 311−315.
(36) Henzie, J.; Kwak, E. S.; Odom, T. W. Mesoscale Metallic Pyramids with Nanoscale Tips. *Nano Lett.* **2005**, *5*, 1199−1202.
(37) Gao, H.; Henzie, J.; Odom, T. W. Direct Evidence for Surface Plasmon-Mediated Enhanced Light Transmission through Metallic Nanohole Arrays. *Nano Lett.* **2006**, *6*, 2104−2108.
(38) Fan, F. J.; Voznyy, O.; Sabatini, R. P.; Bicanic, K. T.; Adachi, M. M.; McBride, J. R.; Reid, K. R.; Park, Y. S.; Li, X. Y.; Jain, A.; Quintero-Bermudez, R.; Saravanapavanantham, M.; Liu, M.; Korkusinski, M.; Hawrylak, P.; Klimov, V. I.; Rosenthal, S. J.; Hoogland, S.; Sargent, E. H. Continuous-Wave Lasing in Colloidal Quantum Dot Solids Enabled by Facet-Selective Epitaxy. *Nature* **2017**, *544*, 75−79.
(39) Adams, M. J. *An Introduction to Optical Waveguides*; John Wiley & Sons: New York, 1981.
(40) Guo, R.; Hakala, T. K.; Torma, P. Geometry Dependence of Surface Lattice Resonances in Plasmonic Nanoparticle Arrays. *Phys. Rev. B: Condens. Matter Mater. Phys.* **2017**, *95*, 155423.
(41) Kravets, V. G.; Kabashin, A. V.; Barnes, W. L.; Grigorenko, A. N. Plasmonic Surface Lattice Resonances: A Review of Properties and Applications. *Chem. Rev.* **2018**, *118*, 5912−5951.
(42) Klimov, V. I.; Mikhailovsky, A. A.; McBranch, D. W.; Leatherdale, C. A.; Bawendi, M. G. Quantization of Multiparticle Auger Rates in Semiconductor Quantum Dots. *Science* **2000**, *287*, 1011−1013.
(43) Park, Y. S.; Bae, W. K.; Baker, T.; Lim, J.; Klimov, V. I. Effect of Auger Recombination on Lasing in Heterostructured Quantum Dots with Engineered Core/Shell Interfaces. *Nano Lett.* **2015**, *15*, 7319−7328.
(44) Ma, R. M.; Oulton, R. F.; Sorger, V. J.; Zhang, X. Plasmon Lasers: Coherent Light Source at Molecular Scales. *Laser Photonics Rev.* **2013**, *7*, 1−21.
(45) Zhou, W.; Dridi, M.; Suh, J. Y.; Kim, C. H.; Co, D. T.; Wasielewski, M. R.; Schatz, G. C.; Odom, T. W. Lasing Action in Strongly Coupled Plasmonic Nanocavity Arrays. *Nat. Nanotechnol.* **2013**, *8*, 506−511.
(46) Empedocles, S. A.; Neuhauser, R.; Bawendi, M. G. Three-Dimensional Orientation Measurements of Symmetric Single Chromophores Using Polarization Microscopy. *Nature* **1999**, *399*, 126−130.
(47) Koberling, F.; Kolb, U.; Philipp, G.; Potapova, I.; Basche, T.; Mews, A. Fluorescence Anisotropy and Crystal Structure of Individual Semiconductor Nanocrystals. *J. Phys. Chem. B* **2003**, *107*, 7463−7471.
(48) Klimov, V. I. Optical Nonlinearities and Ultrafast Carrier Dynamics in Semiconductor Nanocrystals. *J. Phys. Chem. B* **2000**, *104*, 6112−6123.
(49) Adachi, M. M.; Fan, F. J.; Sellan, D. P.; Hoogland, S.; Voznyy, O.; Houtepen, A. J.; Parrish, K. D.; Kanjanaboos, P.; Malen, J. A.; Sargent, E. H. Microsecond-Sustained Lasing from Colloidal Quantum Dot Solids. *Nat. Commun.* **2015**, *6*, 8694.
(50) Carbone, L.; Nobile, C.; De Giorgi, M.; Sala, F. D.; Morello, G.; Pompa, P.; Hytch, M.; Snoeck, E.; Fiore, A.; Franchini, I. R.; Nadasan, M.; Silvestre, A. F.; Chiodo, L.; Kudera, S.; Cingolani, R.; Krahne, R.; Manna, L. Synthesis and Micrometer-Scale Assembly of Colloidal Cdse/Cds Nanorods Prepared by a Seeded Growth Approach. *Nano Lett.* **2007**, *7*, 2942−2950.
(51) Lide, D. R. *CRC Handbook of Chemistry and Physics*; CRC Press: Boca Raton, 2004.

https://dx.doi.org/10.1021/acsnano.9b09466
ACS Nano XXXX, XXX, XXX−XXX